AQUA
Water Infrastructure, Ecosystems and Society

IWA PUBLISHING

 AQUA — Water Infrastructure, Ecosystems and Society Vol 71 No 10, 1229 doi: 10.2166/aqua.2022.234

Transient characteristics during start-up of dual pumps in the prefabricated pumping station

Qing Li[a], Rui Zhang[b,*] and Can Kang[c]

[a] College of Water Conservancy and Hydropower Engineering, Hohai University, Nanjing 210098, China
[b] College of Agricultural Science and Engineering, Hohai University, Nanjing 211100, China
[c] School of Energy and Power Engineering, Jiangsu University, Zhenjiang 212013, China
*Corresponding author. E-mail: gulie1984@163.com

RZ, 0000-0002-1434-9970

ABSTRACT

This work presents a numerical analysis of transient flow fields in the prefabricated pumping station with two identical pumps to clarify the flow evolution process during the start-up using the computational fluid dynamics (CFD) technique. The disturbance between neighboring components and external characteristics of the pump were analyzed and compared. The results demonstrate that the increase of pump head can be divided into two stages: lagging behind the increase of impeller speed and rapid increase of pump head. There is apparent interference between the two pumps, which not only affects the internal flow field distribution of the prefabricated pump station but also severely impacts the pump's performance. The transient impact during the pump start-up threatens the safety of the components of the prefabricated pump station, and the interaction between the pumps causes the pump to deviate from the design working condition. The investigation of results of the complex flow in the prefabricated pumping station during start-up is of great reference to improving the design of the prefabricated pumping station.

Key words: computational fluid dynamics, instantaneous characteristics, mutual interference, prefabricated pumping station, solid-liquid two-phase flow, start-up process

HIGHLIGHTS

- The transient flow pattern during the start-up of the dual pumps in the prefabricated pumping station is revealed.
- The mutual interference between the operation of the dual pumps in the prefabricated pumping station is demonstrated.
- The three stages of the sedimentation of solid particles in the prefabricated pumping station are proposed.

GRAPHICAL ABSTRACT

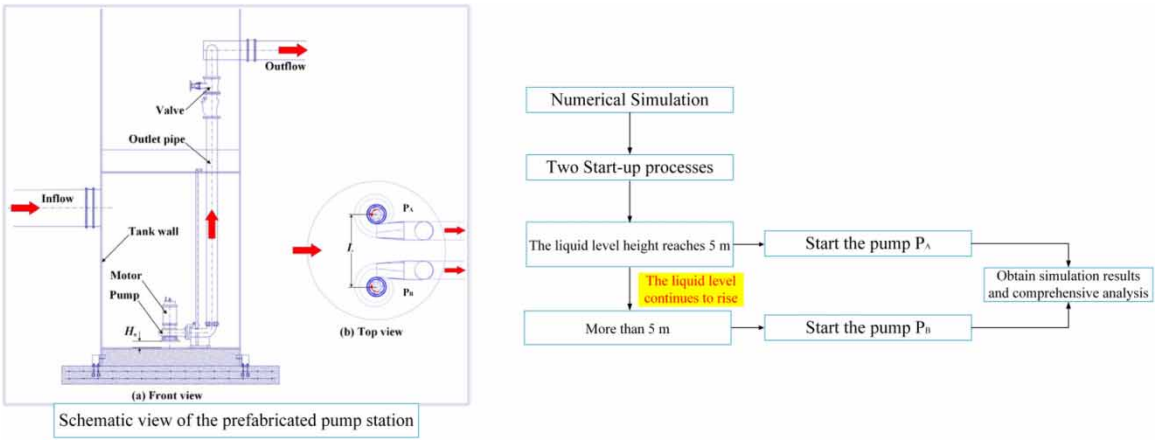

INTRODUCTION

The prefabricated pumping station featuring a relatively new structure plays an essential role in constructing new rural drainage facilities and managing waterlogging in urban areas (Hsu *et al.* 2013; Zeferino *et al.* 2017). The prefabricated pumping station comprises a storage tank, single or multiple pumps, pipes, and various fittings. Typically, two identical pumps will be installed in the prefabricated pumping station. The prefabricated pump station's diameter and height are generally less than 4 m and 12 m due to the limitation of transportation conditions, respectively. The restricted space of the tank constrains the internal flow of the prefabricated pump station. A disturbance between neighboring components is inevitable (Olszewski 2016; Li *et al.* 2019).

In recent years, with the continuous expansion of the application scope of the prefabricated pump station, the internal flow characteristics have been concerned extraordinarily. Based on the CFD results, Zhang *et al.* (2021) found that the geometric installation parameters of pumps had an impact on the hydraulic performance of the prefabricated pump stations. Wang *et al.* (2020) used the discrete phase model (DPM) to study the influence of the suspension height and interval of the pumps on the deposition performance of a prefabricated pump station and proposed the deposition rate and area ratio of the easy deposition region to evaluate the anti-deposition performance. But so far, the existing research literature has been focused on revealing the hydraulic performance of a prefabricated pumping station under steady operation. The liquid level in the prefabricated pumping station constantly fluctuates, resulting in the frequent start and stop of the transport pump. Enough consideration should be paid to the transient start-up process in the prefabricated pumping station. The complex operation mode of the prefabricated pump station is the main factor affecting the performance of the transfer pump. During the start-up of the pump, the drastic variation of the external characteristic parameters of the pump, such as flow rate and head, may cause unstable flow. The internal flow in the prefabricated pumping station responds rapidly to the pump rotational speed due to the effect of flow involvement. Remarkably, one pump is started during the operation of the other pump. The intricate flow structures in the prefabricated pump station are of high possibility.

However, it is not easy to detect the internal flow field with optical flow measurement technology, given the complex structure of the prefabricated pump station. Nevertheless, the experimental research on the pump, especially the research on the starting characteristics of the pump, can provide a reference for this study. Fu *et al.* (2020) investigated the axial flow pump's flow behaviors and transient characteristics during start-up. They found the unstable flow in the impeller and guide vane area and the instantaneous impact characteristics remarkable. This unsteady flow may also arise during the start-up of the prefabricated pump station. Transient behaviors of a centrifugal pump during rapid start-up was experimentally investigated by Tanaka *et al.* (2021) and illustrated that the time-dependent flow field change in several stages. Alternatively, the CFD technique could reveal the evolution process of internal flow structure and the variation of external characteristic parameters (Li *et al.* 2018; Barrios *et al.* 2019; Liu *et al.* 2021). The VLES model was used to simulate the dominant vortex structure (horn-like vortex) in an axial flow pump by Zhao *et al.* (2021). Wang *et al.* (2022) simulated gas-liquid two-phase flow using a volume of fluid (VOF) mathematical model. Li *et al.* (2020) obtained the effect of the distorted inflow condition on the performance of a reactor coolant pump numerically. They experimentally verified that the computational fluid dynamics (CFD) technique could be employed in performance predictions. Furthermore, the coupling of the discrete element method (DEM) and the CFD technique has been attempted to multiphase fluid flow.

Moreover, different from the study of the transient characteristics of an impeller pump independently starting, interaction mechanisms of the internal flow field of multi-flow passage components in a prefabricated pumping station have rarely been reported. The prefabricated pumping station is a drainage system comprised of multiple components, among which imparity in flow characteristics is remarkable. It may cause mutual interference between the operation of the two pumps. Especially in the transportation of sewage, sedimentation may occur in the prefabricated pumping station. The instantaneous impact characteristics during start-up may affect the stability of the pump station operation.

The emphasis of the presented work is concerned with the complex flows in a prefabricated pumping station that allows transporting the solid-liquid two-phase medium. Unsteady numerical simulations were performed for the start-up of the prefabricated pumping station under two different start-up conditions, namely the start-up of the pump P_A and the start-up of the pump P_B during the operation of the pump P_A. Time-dependent variation of the pump performance and instantaneous flow characteristics of the prefabricated pumping station during the start-up of the two pumps were described. Solid-liquid two-phase medium parameter distributions, and interference between two pumps, were investigated comprehensively. Instantaneous flow features during the start-up of the two pumps in the prefabricated pumping station were analyzed. The present study aims to reveal transient characteristics in a prefabricated pumping station during start-up.

METHODOLOGY

Prefabricated pumping station model

Two identical pumps are symmetrically mounted in the storage tank, as shown in Figure 1. The horizontal distance between the two pump axes, L, is 2,000 mm. The vertical distance between the pump inlet section and the tank bottom, H_0, which represents the mounting height of the two pumps, is 200 mm. The diameter of the tank, D, is fixed at 3,800 mm. The nominal flow rate of each pump is 1,940 m^3/h, and the pump head of 11.0 m is attainable at the nominal flow rate and the rotational speed of 740 rpm. The pump is kept submerged in the two-phase medium. The complex flow characteristics in the prefabricated pumping station are mainly investigated. Therefore, joint and auxiliary parts, such as interface flange and valve, are omitted to simplify the calculation model. The pump, storage tank, pipe, and other over-current components are assembled to form a three-dimensional model of the calculation domain, as shown in Figure 2.

Start-up process

Two different kinds of start-up conditions are established according to the liquid level height in a prefabricated pumping station. Only the pump P_A is started when the liquid level height reaches 5 m. If the liquid level in the prefabricated pump station continues to rise by more than 5 m, the pump P_B is required to start, namely the start-up of the pump P_B during the operation of the pump P_A. Therefore, the starting initial conditions of the pump P_B in the prefabricated pump station differ from those of the pump P_A. The nominal speed of the pump, n, is 740 rpm, and 2.2 s, Ttol, is needed from starting acceleration to nominal speed, and the acceleration process is linear (Li *et al.* 2011). The equation for the rotation speed of the pump and the start-up time is written as:

$$n(t) = n_0 + \frac{n - n_0}{T_{tol}} t \tag{1}$$

where n_0 is the initial rotation speed, t represents the start-up time.

Governing equations and turbulence model

The solid-liquid two-phase flow in the prefabricated pumping station is assumed as a three-dimensional incompressible flow and follows the law of physical conservation (Song *et al.* 2019). The flow was governed by Reynolds-averaged Navier-Stokes (RANS) equations (Winardi *et al.* 2018). The continuity equations for the liquid phase and the solid phase can be written respectively as:

$$\frac{\partial}{\partial t}(\rho_l \phi_l) + \nabla(\rho_l \phi_l \overrightarrow{u_l}) = 0 \tag{2}$$

$$\frac{\partial}{\partial t}(\rho_s \phi_s) + \nabla(\rho_s \phi_s \overrightarrow{u_s}) = 0 \tag{3}$$

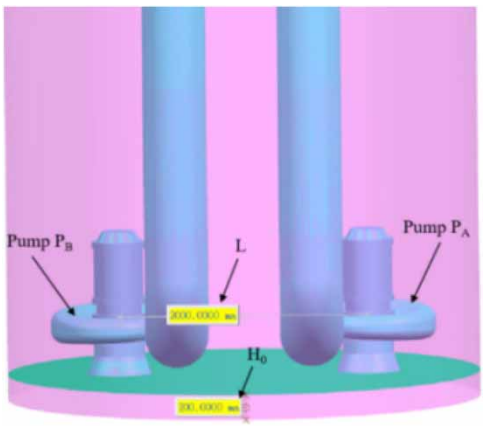

Figure 1 | Layout of two pumps in the prefabricated pumping station.

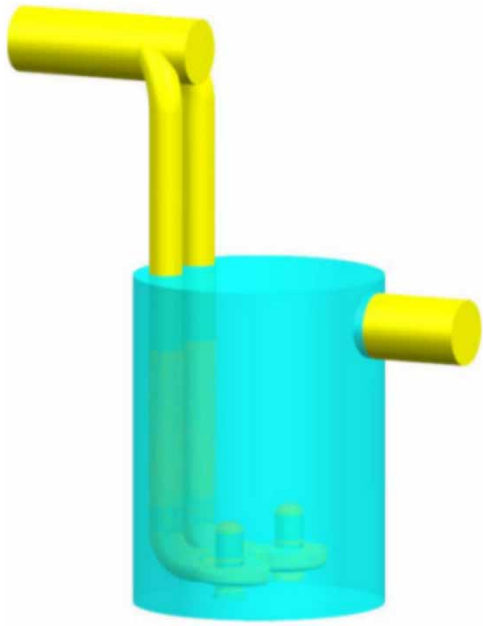

Figure 2 | Computation domains for the prefabricated pumping station.

where the subscript l represents liquid phase and s solid phase; φ is the volume fraction; ρ is the density; $\vec{u}$ is the velocity.

The momentum equation is expressed as:

$$\frac{\partial}{\partial t}(\phi_s \rho_s \overrightarrow{u_s}) + \nabla(\phi_s \rho_s \overrightarrow{u_s}\,\overrightarrow{u_s}) = -\phi_s \nabla P - \nabla P_s + \nabla \tau_s + \phi_s \rho_s g + K_{ls}(\overrightarrow{u_l} - \overrightarrow{u_s}) \tag{4}$$

$$\frac{\partial}{\partial t}(\phi_l \rho_l \overrightarrow{u_l}) + \nabla(\phi_l \rho_l \overrightarrow{u_l}\overrightarrow{u_l}) = -\phi_s \nabla P + \nabla \tau_l + \phi_l \rho_l g + K_{sl}(\overrightarrow{u_s} - \overrightarrow{u_l}) \tag{5}$$

where τ is stress tensor, K_{ls} and K_{sl} are momentum transfer coefficients, P_s is particulate phase pressure.

The standard k–ε turbulence model was selected for turbulence modeling to accomplish the closure of RANS equations, and standard wall functions were used to treat near-wall flows (Balakin *et al.* 2011). The standard k–ε turbulence model can accurately predict the complex flow patterns inside the prefabricated pumping station. The Eulerian-Eulerian model was employed as the multiphase flow model (Shi *et al.* 2010; Ahmadkermaj *et al.* 2020). Such a multiphase flow model has been widely used to simulate solid-liquid two-phase flows. The Eulerian-Eulerian model can fully simulate the turbulent transport of solid particles and obtain the detailed spatial distribution of solid particles (Kaushal *et al.* 2012). The Eulerian-Eulerian model can describe the influence of particle inertia on particle gravity flow, including the flow structure and dynamic characteristics of particle gravity flow. This model also applies to the sedimentation of a non-Brown sphere with uniform size in a viscous fluid. A good agreement of computed results with this model and experimental data is observed (Messa *et al.* 2015).

Boundary conditions

Based on practical requirements, the mixture of water and sand particles with a mean diameter of 0.5 mm was selected as the solid-liquid two-phase medium to be transported. The density of sand particles was 2,300 kg/m^3. The volume fraction possessed by the solid phase in the mixture was set as 3%. At the inlet of the prefabricated pumping station, the velocity inlet boundary conditions were imposed. Liquid velocity magnitude was calculated with the designated flow rate and the inlet area. Velocities of the two phases were set as equivalent and uniformly distributed over the inlet section. For the two start-up modes, the inflow rate of 1,940 m^3/h was selected for the start-up of the pump P_A, and the inflow rate of 3,880 m^3/h was selected for the start-up of the pump P_B during the operation of the pump P_A. At the outlet of the

prefabricated pumping station, constant static pressure at local atmospheric pressure was defined, and the flow direction was perpendicular to the outlet section (Kang *et al.* 2020). The time step of the unsteady numerical simulation was set to 0.0022 s, which was demonstrated to sufficiently capture the flow process in such pump arrangements.

Grid independence study

The commercial software of ANSYS ICEM was used to execute grid generation. The prefabricated pumping station comprises multiple components that vary significantly in size and geometry. Therefore, unstructured grids were adopted to discretize the computational domain spatially. A grid refinement was implemented at the connection with a significant size difference to improve the accuracy of numerical simulation. Grids for the computational domain are illustrated in Figure 3. More detailed information can be found in Kang *et al.* (2020).

To eliminate the uncertainty possibly caused by insufficient grid numbers on the numerical simulation results, seven sets of grids with numbers ranging from about 4.75 to 8.19 million were selected to evaluate the dependence of the pump head on the pump P_A, and the solid-phase concentration averaged over the inlet section of the pump P_A on the grid resolution. The corresponding results are listed in Table 1 (Kang *et al.* 2020). As the grid number exceeded 724 million, the gap between adjacent pump heads or solid-phase concentrations is below 2%. Therefore, Grid scheme E was adopted in the current simulations.

RESULTS AND DISCUSSION

Forces exerted on solid particles

Solid particles in the flow field are subject to a combination of forces from themselves and the flow field, resulting in energy and momentum transfer between the solid and liquid phases, including gravity, pressure gradient force, inertial force,

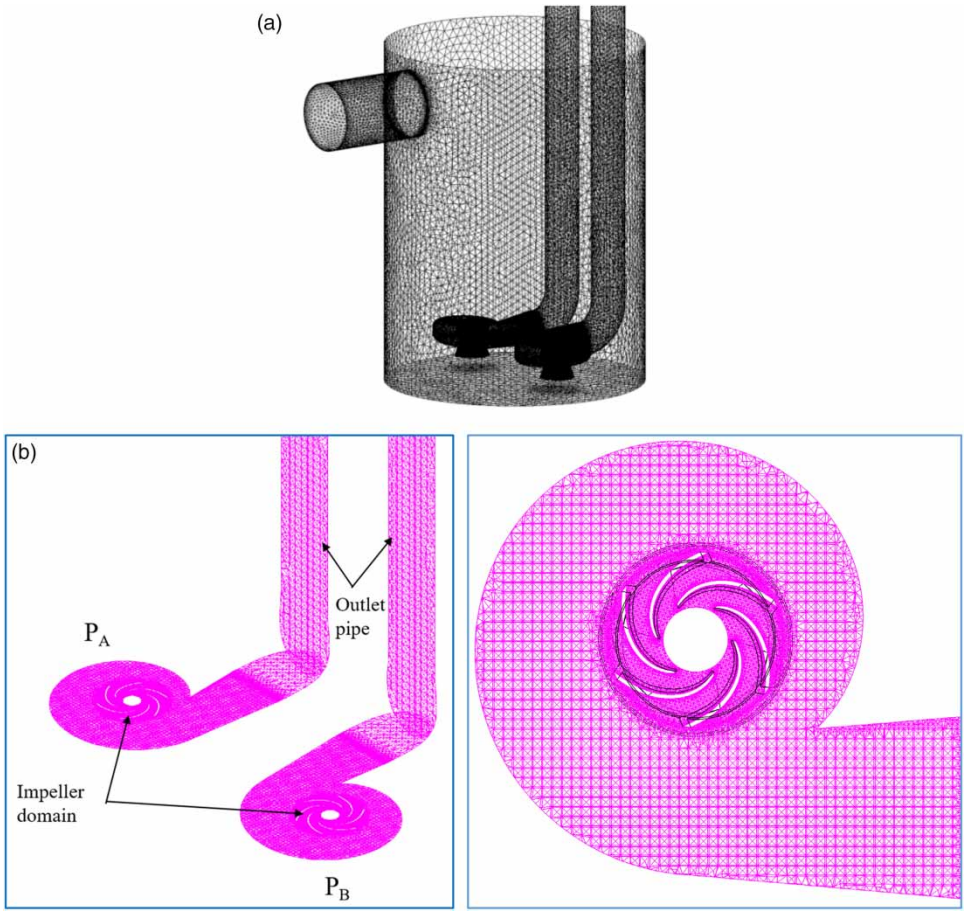

Figure 3 | Grids for the computation domain. (a) Grids for the whole computational domain. (b) Local grids.

Table 1 | Grid independence analysis

Grid Scheme	Grid number	Pump head (m)	Solid-phase concentration
A	4751253	11.25	0.0278
B	5253060	11.22	0.0292
C	5847192	11.30	0.0286
D	6719423	11.33	0.0289
E	7240635	11.36	0.0293
F	7753696	11.35	0.0297
G	8185318	11.37	0.0293

resistance force, and Mangus force. Gravity and inertial forces are independent of the relative motion between the solid and liquid phases. Still, they play a significant role in the suspension and deposition of solid particles in the flow field. Resistance and Magnus force are produced by the relative motion between the solid and the liquid phases. The resistance is due to the relative motion between the solid and liquid phases, which results from the fluid's viscosity. Magnus force perpendicular to the relative velocity of particles and fluid is generated by the rotation of particles in the flow field. The four forces mentioned above cannot be neglected because of their significant influence on the movement of particles in the flow field. Under the combined action of these forces, the distribution of solid particle velocity in the vertical direction was plotted in Figure 4, based on the numerical results obtained. The solid particle velocity in the vertical direction was averaged over each monitored cross-section when the pump P_A and the pump P_B simultaneously operated at the design speed and flow rate. Figure 4 reveals three stages of the sedimentation of solid particles in the prefabricated pumping station, i.e., the acceleration stage, the rather stable stage, and the sharp drop stage.

Distributions of solid-phase concentration in the pump

During the start-up of the pump P_A, the solid-phase concentration distribution on the pressure and suction surfaces of the blades is displayed in Figure 5. The impeller rotational speed corresponding to the four times in the figure are 185, 370, 555, and 740 rpm, respectively. The pump is the only equipment that transfers energy to the transported medium in the prefabricated pumping station. As the rotation speed of the pump increases, more and more solid particles are sucked into the pump. Therefore, the solid-phase concentration on the blade rises gradually. The solid-phase concentration on the blade pressure surface is consistently higher than its counterpart on the blade suction surface. The possibility of blade pressure

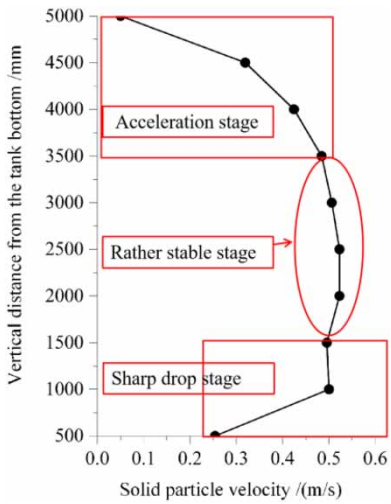

Figure 4 | Variations of the solid particle velocity in vertical direction.

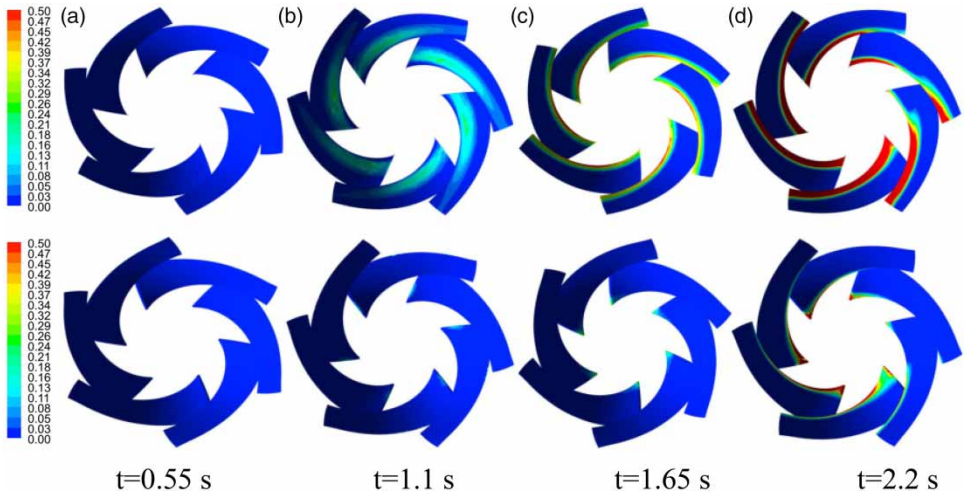

Figure 5 | Distributions of solid-phase concentration over the blade pressure surface (above) and suction surface (below). (a) t = 0.55 s. (b) t = 1.1 s. (c) t = 1.65 s. (d) t = 2.2 s.

surface wear is greater than the suction surface. It can be expected that the same phenomenon will occur during the start-up of the pump P_B.

Time-dependent variations of the pump head

The start-up of a prefabricated pumping station is a process in which the pump rotational speed increases with time, and the external characteristic parameters of the pump change accordingly. Time-dependent variation of the pump head during the start-up was described in Figure 6. As for the start-up of the pump P_A, as shown in Figure 6(a), the pump head presents two prominent rising stages with the increase of the rotational speed. At the initial stage of start-up, the pump head rises slowly with slight fluctuations. In contrast, the pump head rises sharply to the maximum value in 0.4 seconds. The maximum pump head satisfies the design requirements. In the second stage, the pump head increased by nearly 73% relative to the maximum head. There is a risk of damaging the drainage system (Meng *et al.* 2021).

As for the start-up of the pump P_B during the operation of the pump P_A, as shown in Figure 6(b). It is noticeable that the pump head changes irregularly during the first 0.22 seconds of the pump P_B start-up, as shown in Figure 6(c). As the rotational speed of the pump P_B increases, the pump head changes to a more regular increase. It is apparent that the pump P_B is susceptible to interference from the operation of the pump P_A when the speed is low. The head change during the start-up process of the pump P_B is gentler, and there is no apparent mutation, so the instantaneous impact on the head is weak. However, the pump P_B starts with a maximum head of 13 m, nearly 18% higher than the design head. It can be clearly reflected in Figure 6 that at the initial start-up stage, the growth rate of the pump head growth rate is less than that of impeller rotation speed. Therefore, it can be concluded that the pump head's response velocity lags behind the impeller rotation acceleration.

Distributions of the velocity and streamlines

The internal flow field of the prefabricated pump station varies instantaneously with the increase of pump rotation speed during the start-up. At two different start-up conditions, distributions of the velocity and streamlines of the liquid phase in the tank section at the pump suction are plotted in Figure 7. As for the start-up of the pump P_A, the flow velocity in the prefabricated pump station is slow. Near the pump inlet, a relatively high velocity is caused by the rotation of the pump impeller. Although the flow velocity of the liquid phase on the section is small in the initial stage of pump start-up, the degree of freedom of motion in the spacious tank is remarkably high, and the flow in the tank is disordered, which can be informed by observing the streamlines distribution on the section (Leporini *et al.* 2019). It is noticeable that the above and below sides in the section are distinguished evidently by considerably different flow patterns. The pump's suction capacity is enhanced, and the internal flow field of the prefabricated pump station is restrained and tends to flow into the pump P_A due to the pump rotation speed increasing.

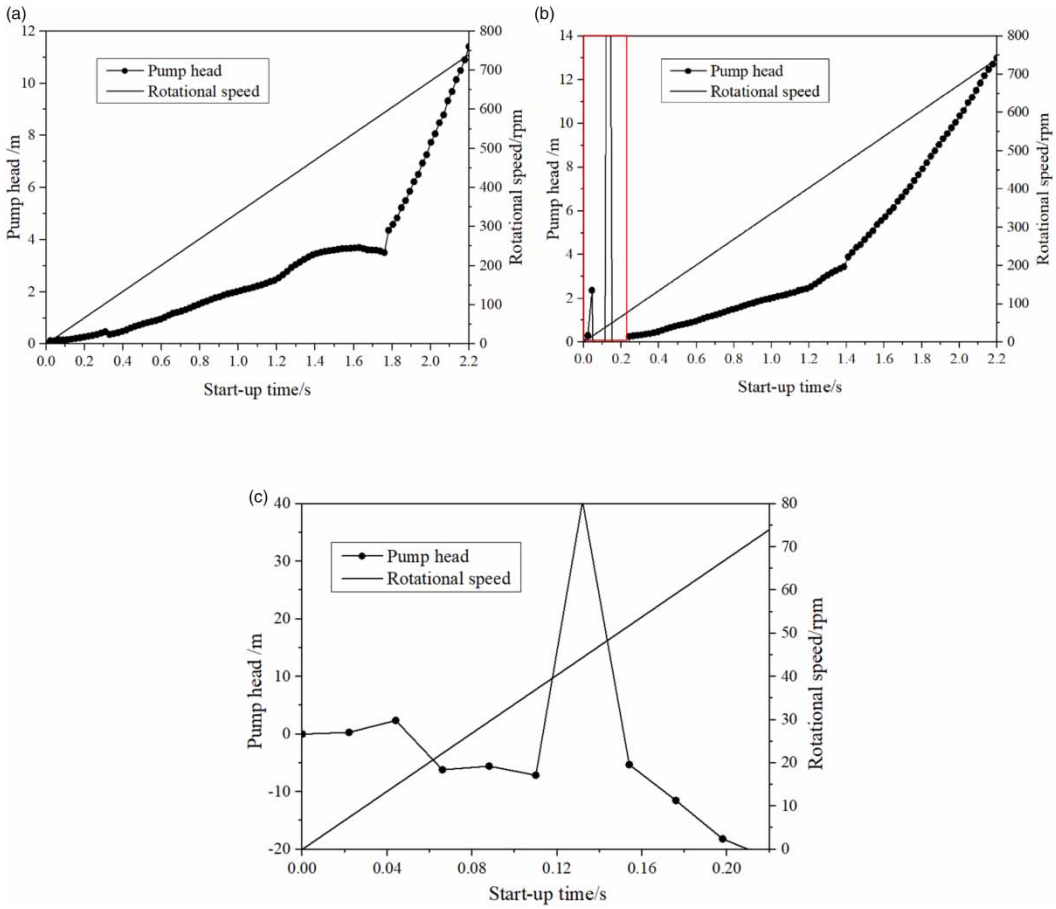

Figure 6 | Time-dependent variations of the pump head during the pump start-up. (a) Start-up of the pump P_A. (b) Start-up of the pump P_B. (c) First 0.22 s of the pump P_B start-up.

As for the start-up of the pump P_B during the operation of the pump P_A, the velocity of the liquid phase near the pump P_A inlet is exceptionally high overall. In the pump P_B start-up process, the liquid phase's velocity near the pump suction gradually increases, and the flow velocity presents the same rule as that of pump P_A start-up. However, the velocity uniformity on the section near the inlet of the pump P_A is destroyed. It is further revealed that there is mutual interference between the two pumps. In the first 0.55 s of the pump P_B start-up, the flow of the section is featured by uniform distribution, demonstrated by the streamlines. On the one hand, due to the more substantial suction capacity of the pump P_A, the medium mainly flows to the pump P_A at this moment. On the other hand, with the gravity effect, pump P_B's rotational speed is insufficient to disturb the flow. The two factors jointly contribute to the uniform flow distribution in the section. Nevertheless, with the increased rotation speed of the pump P_B, the mutual interference between the pump P_B and the pump P_A enhances, thereby destroying the uniform flow. The mutual interference between pumps is the main reason that causes the pump performance to deviate from the design condition and unstable operation.

Distributions of the axial velocity

Solid particle velocity is an essential index of solid-liquid two-phase flow patterns (Uzi & Levy 2018). To describe the motion of sand particles, distributions of the axial velocity at the pump inlet section during the start-up of the pump P_A are displayed in Figure 8(a). Note that the negative velocity signifies that the solid particles are moving toward the bottom of the prefabricated pump station. It is seen that the pumping capacity is not sufficient to fully overcome the gravity of solid particles at the initial stage of start-up. Consequently, the solid particles move towards the bottom of the prefabricated pump station at a relatively low speed, indicating the possible deposition (Zordan *et al.* 2018). With the increase of the pump rotation speed, the

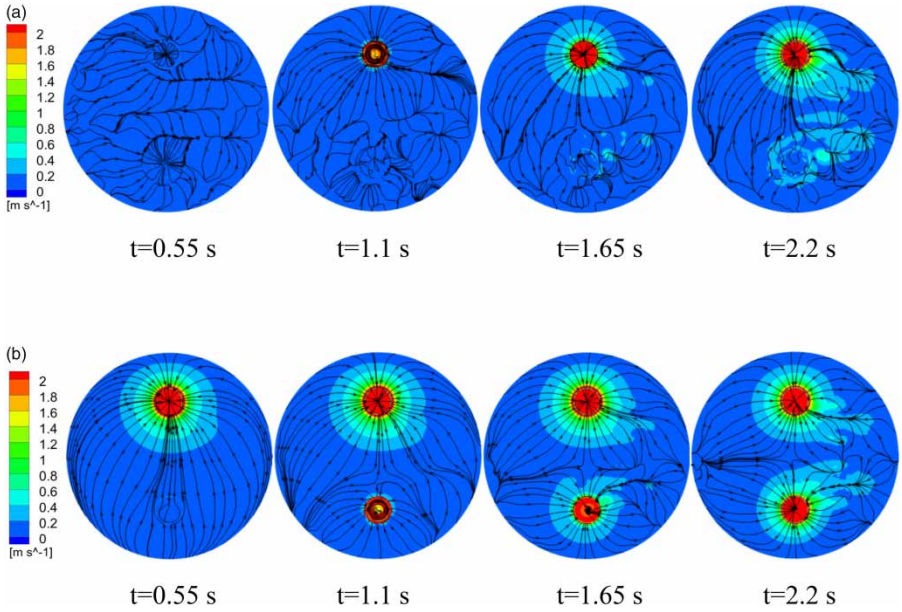

Figure 7 | Distributions of the velocity and streamlines of the liquid phase over the tank section at the pump suction. (a) Start-up of the pump P_A. (b) Start-up of the pump P_B. t = 0.55 s. t = 1.1 s. t = 1.65 s. t = 2.2 s.

medium flow velocity increase after the work of the impeller is absorbed. Therefore, the axial velocity of the solid particles turns to the direction of the pump inlet. It is speculated that the solid particles deposited at the bottom of the storage tank of the prefabricated pump station move into the pump and are transported out of the storage tank. However, near the pump inlet wall, the solid particles still deposit to the bottom of the storage tank as the collision and friction on the wall decrease the kinetic energy of solid particles.

In Figure 8(b), the axial velocity distribution at the pump inlet section during the start-up of the pump P_B is exhibited. The axial suction velocity of the solid particles at the pump inlet is relatively smaller, mainly due to the combined influence of the impeller rotation of the pump P_A and gravity. However, due to the disturbance and dispersion of the solid particles in the storage tank by the pump P_A, when the rotational speed of the pump P_B reaches the nominal rotational speed, the axial velocity of the solid particles at the inlet of the pump P_B is greater than that of the pump P_A. Such a flow pattern mitigates the deposition in the storage tank, which is beneficial for the pump P_B to transport solid particles.

Radial force exerted on the impeller

Variations of the radial force exerted on the impeller during the pump start-up are plotted in Figure 9. Theoretically, the resultant radial force exerted on the impeller should be 0 N due to the circumferential symmetry design of the blade. However, because of the dynamic and static interference between the impeller and the volute, the internal flow of the pump is complex, so the impeller will still be subjected to radial forces.

The two different start-up conditions exhibit the same changing tendency, i.e., the radial force exerted on the fluctuating impeller grows with the pump rotational speed increase. On the one hand, the medium's suction volume increases with the pump's acceleration. On the other hand, the unsteady start-up process of the pump results in an unstable internal flow field. The two factors jointly contribute to the various characteristics of the radial force exerted on the impeller during the start-up process. The difference in the highest radial force exerted on the impeller is significant for two different start-up conditions. At the end of the start-up process, the radial force exerted on the impeller of the pump P_B is reduced by nearly 200 N compared with that on the impeller of the pump P_A.

CONCLUSIONS

In this work, unsteady numerical simulations were performed to investigate the start-up process of the prefabricated pumping station under two different start-up conditions. Time-dependent variation of the pump performance and instantaneous flow characteristics of the prefabricated pumping station during the pump start-up were identified.

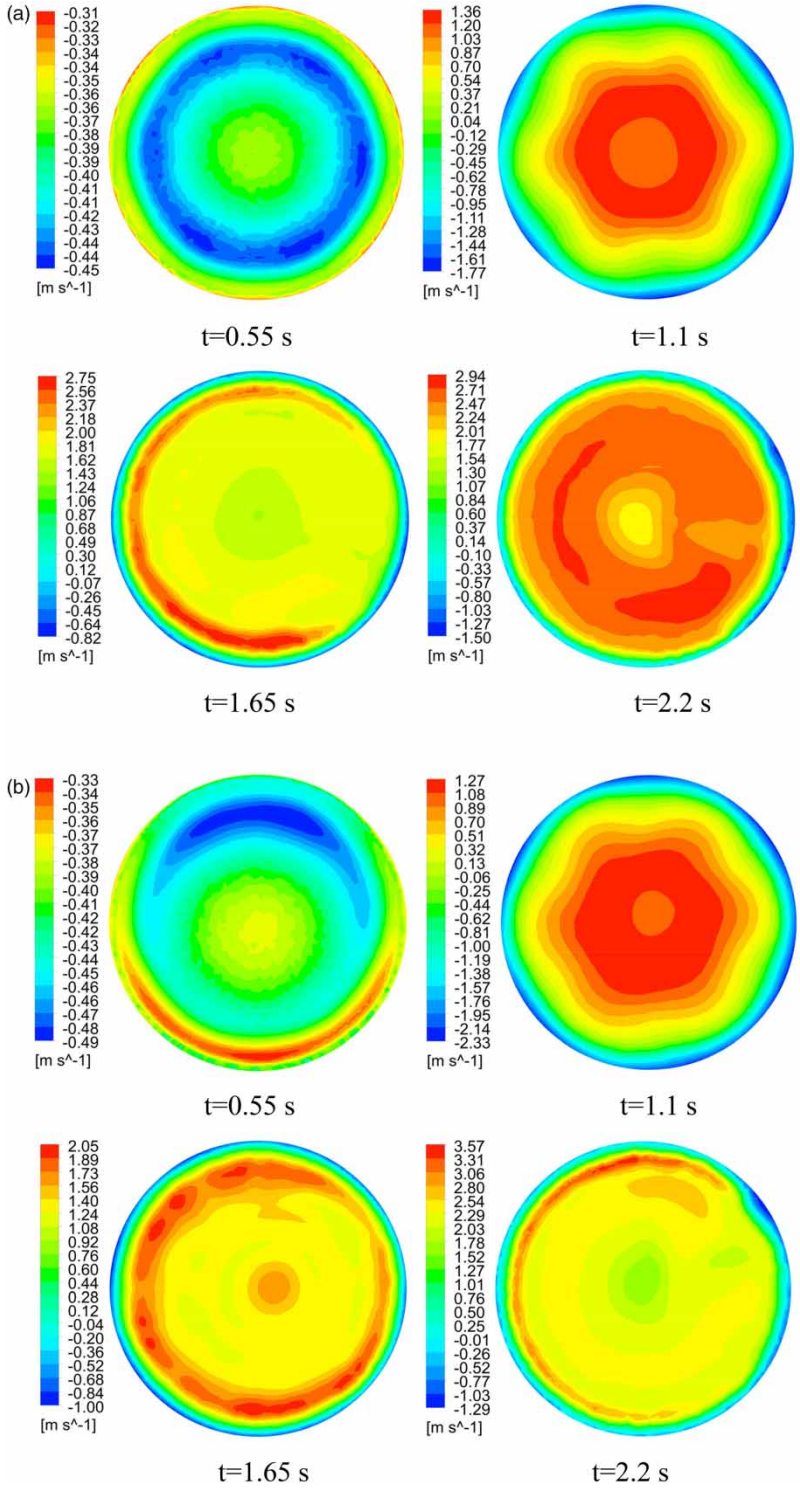

Figure 8 | Distributions of the axial velocity over the pump inlet section. (a) Start-up of the pump P_A. (b) Start-up of the pump P_B.

At the initial start-up stage of two pumps, the response velocity of the increase of the pump head lags behind the acceleration of impeller rotation. There is a transient impact on the head of the pump P_A. The pump P_A head increases sharply by nearly 73% relative to the maximum head from 1.8 s to 2.2 s. The maximum starting head of the pump P_B is 13 m, which

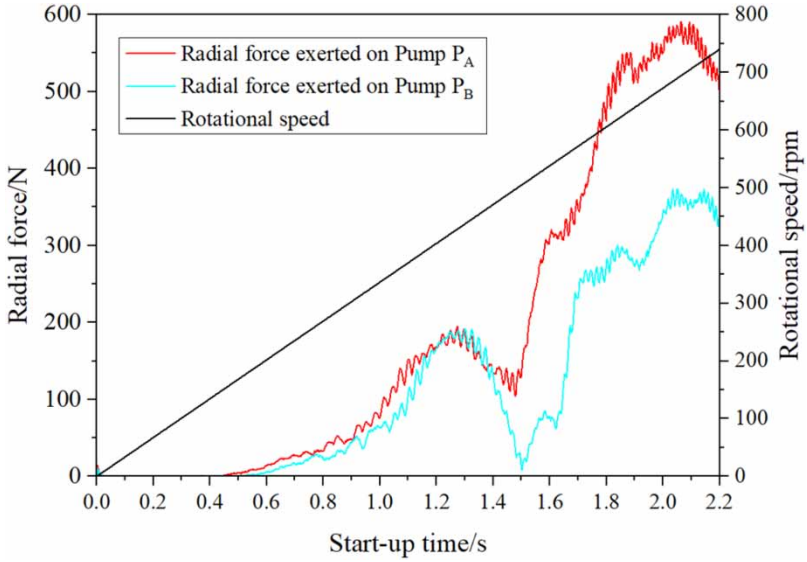

Figure 9 | Variations of the radial force exerted on the impeller during the pump start-up.

exceeds the design head by 18%. The transient impact of the head and the deviation of the maximum head from the design head during start-up may cause damage to the pumps, valves, and pipes, especially when transporting solid-liquid two-phase media. Therefore, the reliability of components should be fully considered in the design of a prefabricated pump station.

Intense disturbance stemming from the pump P_A and the pump P_B operation to the tank's medium is demonstrated. Although the two pumps are symmetrically arranged in the storage tank of the prefabricated pump station, the flow fields formed by the start-up of the pump P_A and the pump P_B are not identical. The pump P_A and pump P_B also have different suction capacities for solid particles during start-up. Meanwhile, the difference in radial force exerted on the two pumps is evident during start-up. The radial force exerted on the impeller of the pump P_B is reduced by nearly 40% compared with that on the impeller of the pump P_A at the end of the start-up process. It indicates that there is apparent interference between the two pumps. Therefore, the inter-pump distance of the two pumps should be reasonably designed to mitigate the interference characteristic.

In this paper, limited by the experimental conditions and methods, only the numerical simulation method is used to qualitatively study the transient flow characteristics during the start-up of dual pumps in prefabricated pump stations. In the follow-up research, on the premise of improving the flow measurement and visualization methods, model experiments can be used to visualize the complex flow in the prefabricated pump station and obtain quantitative research results.

ACKNOWLEDGEMENTS

This study was supported by the National Natural Science Foundation of China (Grant No.51809081), the Natural Science Foundation of Jiangsu Province (Grant No. BK20201315), the China Postdoctoral Science Foundation (Grant No.2019M661707), the Jiangsu Planned Projects for Postdoctoral Research Funds (Grant No.2019K095), and the Science and Technology Plan Project of State Administration for Market Regulation of China (Grant No. 2021MK060).

DATA AVAILABILITY STATEMENT

All relevant data are included in the paper or its Supplementary Information.

CONFLICT OF INTEREST

The authors declare there is no conflict.

REFERENCES

Ahmadkermaj, H., Maddahian, R. & Maerefat, M. 2020 Effect of swirl on thermal and hydraulic properties of ice slurry flow. *Heat Transfer Engineering* **42** (9), 764–786.

Balakin, B. V., Hoffmann, A. C. & Kosinski, P. 2011 Experimental study and computational fluid dynamics modeling of deposition of hydrate particles in a pipeline with turbulent water flow. *Chemical Engineering Science* **66** (4), 755–765.

Barrios, J. A., Solís-Caballero, F. E., Cano, A., Durán, U., Orozcoc, G. & Riverad, F. F. 2019 Two-phase hydrodynamic modelling and experimental characterization in an activated sludge electrooxidation flow reactor. *Chemical Engineering Research and Design* **141**, 339–349.

Fu, S. F., Zheng, Y., Kan, K., Chen, H. X., Han, X. X., Liang, X. L., Liu, H. W. & Tian, X. Q. 2020 Numerical simulation and experimental study of transient characteristics in an axial flow pump during start-up. *Renewable Energy* **146**, 1879–1887.

Hsu, N. S., Huang, C. L. & Wei, C. C. 2013 Intelligent real-time operation of a pumping station for an urban drainage system. *Journal of Hydrology* **489**, 85–97.

Kang, C., Li, Q., Li, M. Y. & Teng, S. 2020 Deposition of solid particles exposed to the suction of dual pumps in the tank of a pumping station. *Powder Technology* **361**, 727–738.

Kaushal, D. R., Thinglas, T., Yuji, T., Shigeru, K. & Hiroshi, T. 2012 CFD modeling for pipeline flow of fine particles at high concentration. *International Journal of Multiphase Flow* **43**, 85–100.

Leporini, M., Terenzi, A., Marchetti, B., Corvaro, F. & Polonara, F. 2019 On the numerical simulation of sand transport in liquid and multiphase pipelines. *Journal of Petroleum Science and Engineering* **175**, 519–535.

Li, Z. F., Wu, P., Wu, D. Z. & Wang, L. Q. 2011 Experimental and numerical study of transient flow in a centrifugal pump during start-up. *Journal of Mechanical Science & Technology* **25** (3), 749–757.

Li, G. H., Li, Z. P., Gao, Z. M., Wang, J. W., Bao, Y. Y. & Derksenc, J. J. 2018 Particle image velocimetry experiments and direct numerical simulations of solids suspension in transitional stirred tank flow. *Chemical Engineering Science* **191**, 288–299.

Li, Q., Kang, C., Teng, S. & Li, M. Y. 2019 Optimization of tank bottom shape for improving the anti-deposition performance of a prefabricated pumping station. *Water* **11** (3), 602–602.

Li, Y. B., Fan, Z. J., Guo, D. S. & Li, X. B. 2020 Dynamic flow behavior and performance of a reactor coolant pump with distorted inflow. *Engineering Applications of Computational Fluid Mechanics* **14** (1), 683–699.

Liu, Y., Wang, D. Z. & Ran, H. J. 2021 Computational research on the formation mechanism of double humps in pump–turbines. *Engineering Applications of Computational Fluid Mechanics* **15** (1), 1542–1562.

Meng, L., Wang, W. P., Liao, C. L., Zhao, L. C., He, L. & Zhang, C. Y. 2021 Non-dimensional study on the start-up process of a centrifugal pump and its related pipe system. *IOP Conference Series: Earth and Environmental Science* **627** (1), 012006.

Messa, G. V., Ferrarese, G. & Malavasi, S. 2015 A mixed Euler–Euler/Euler–Lagrange approach to erosion prediction. *Wear* **342-343**, 138–153.

Olszewski, P. 2016 Genetic optimization and experimental verification of complex parallel pumping station with centrifugal pumps. *Applied Energy* **178**, 527–539.

Shi, D. P., Luo, Z. H. & Zheng, Z. W. 2010 Numerical simulation of liquid-solid two-phase flow in a tubular loop polymerization reactor. *Powder Technology* **198** (1), 135–143.

Song, Y. H., Yun, R., Lee, E. H. & Lee, J. H. 2019 Predicting sedimentation in urban sewer conduits. *Water* **10** (4), 462.

Tanaka, T., Toyomoto, T., Nasu, K. & Tabaru, M. 2021 Transient characteristics of a centrifugal pump at rapid start-up. *Journal of Physics: Conference Series* **1909** (1), 012032. doi.10.1088/1742-6596/1909/1/012032.

Uzi, A. & Levy, A. 2018 Flow characteristics of coarse particles in horizontal hydraulic conveying. *Powder Technology* **326**, 302–321.

Wang, K., Bao, H. F., Liu, H. L., Zhang, Z. X. & Hu, J. B. 2020 Influence of the installation position of submersible pumps on deposition characteristics in prefabricated pumping stations. *Symmetry* **12** (8), 1347.

Wang, Y. R., Yu, X. D., Qin, H. X., Cheng, N. & Yu, C. 2022 Analysis of pressure surges for water filling in deep stormwater storage tunnels with entrapped air-pocket using a VOF model. *AQUA-Water Infrastructure, Ecosystems and Society* **71** (9), 992–1001. doi:10.2166/aqua.2022.039.

Winardi, S., Widiyastuti, W., Septiani, E. L. & Nurtono, T. 2018 Simulation of solid-liquid flows in a stirred bead mill based on computational fluid dynamics (CFD). *Materials Research Express* **5** (5), 054002.

Zeferino, J. A., Cunha, M. C. & Antunes, A. P. 2017 Adapted optimization model for planning regional wastewater systems: case study. *Water Science & Technology* **76** (5), 1196–1205.

Zhang, B., Cheng, L., Xu, C. & Wang, M. 2021 The influence of geometric parameters of pump installation on the hydraulic performance of a prefabricated pumping ptation. *Energies* **14**, 1039.

Zhao, H. R., Wang, F. J., Wang, C. Y., Chen, W. H., Yao, Z. F., Shi, X. Y., Li, X. Q. & Zhong, Q. 2021 Study on the characteristics of horn-like vortices in an axial flow pump impeller under off-design conditions. *Engineering Applications of Computational Fluid Mechanics* **15** (1), 1613–1628.

Zordan, J., Juez, C., Schleiss, A. J. & Franca, M. J. 2018 Image processing and laser measurements for determination of the erosion and deposition of fine sediments by a gravity current. *Measurement Science & Technology* **29** (6), 065905.

First received 10 August 2022; accepted in revised form 2 October 2022. Available online 12 October 2022